IEEE Access
Multidisciplinary | Rapid Review | Open Access Journal

Received October 1, 2020, accepted October 14, 2020, date of publication October 19, 2020, date of current version October 30, 2020.

Digital Object Identifier 10.1109/ACCESS.2020.3032132

Low Loss Substrate-Integrated Waveguide Using 3D-Printed Non-Uniform Honeycomb-Shaped Material

YEONJU KIM AND SUNGJOON LIM, (Member, IEEE)
School of Electrical and Electronics Engineering, Chung-Ang University, Seoul 06974, South Korea

Corresponding author: Sungjoon Lim (sungjoon@cau.ac.kr)

This work was supported in part by the Chung-Ang University Graduate Research Scholarship in 2014, and in part by the National Research Foundation of Korea (NRF) funded by the Ministry of Science, ICT and Future Planning (MSIP), Korea Government under Grant 2017R1A2B3003856.

ABSTRACT Despite the low cost and easy fabrication afforded by 3D printing technology, high dielectric loss of the 3D printing filament degrades the performance of 3D printed radio frequency electronics at high frequencies. In this paper, we propose a 3D-printed substrate-integrated waveguide (SIW) using a lossy polylactic acid or polylactide (PLA) filament. To minimize the insertion loss of the SIW, a non-uniform honeycomb is 3D-printed as the dielectric material of the SIW. The non-uniform honeycomb-shaped substrate is composed of large unit cells, which achieve low insertion loss (0.01 dB/mm) because of the low volume of the dielectric material. The performance characteristics of the proposed SIW is compared with those of SIWs made of solid and uniform honeycomb-shaped structures. The average insertion loss of the microstrip line-fed SIW with the proposed non-uniform honeycomb substrate is 0.92 dB in the frequency range of 1.97 to 3.35 GHz and those of the solid PLA and uniform honeycomb substrates are 2.49 dB and 1.38 dB, respectively. The proposed 3D-printed SIW additionally has the advantages of light weight and low cost.

INDEX TERMS 3D printing, polylactic acid, non-uniform honeycomb substrate, substrate integrated waveguide.

I. INTRODUCTION

Three-dimensional (3D) printing technology, which is also known as "additive manufacturing", is used to create 3D objects with computer-aided design data by depositing successive layers of materials. This innovative manufacturing process enables the rapid, cost-effective, and environmentally friendly production of prototypes without by-products compared to conventional subtractive manufacturing [1]–[3]. Moreover, 3D printing technology supports design and material flexibility; it can be applied in a wide range of research areas. For example, bionic ears have been created with 3D printing technology for biological tissue mimicking [4]. Furthermore, by using 3D printing technology, microfluidic devices [5] and electrochemical energy storage devices with highly resolved nanostructures and optimal performance characteristics have been fabricated [6].

The associate editor coordinating the review of this manuscript and approving it for publication was Kuang Zhang.

Microwave devices have been developed with various manufacturing technologies to obtain inexpensive, lightweight, and easily integrable devices. Traditionally, radio frequency (RF) and microwave components are fabricated by machining printed circuit boards (PCB) [7]–[10] and using low-temperature cofired ceramic (LTCC) technology [11]. Because the performance characteristics of passive RF and microwave devices are closely related to the dielectric properties of the substrate materials, LTCC technology has been used to reduce the dielectric loss of the substrate and obtain microwave devices with good performance characteristics [12]. By combining many thin layers of ceramic and conductive metal paste, LTCC technology allows the implementation of multilayer stacked devices with low losses and compact sizes [13], [14]. In addition, the technology enables integrated circuit packaging and passive microwave component integration. However, LTCC technology involves complex fabrication processes and carefully selected materials.

By contrast, 3D printing technology has a simple manufacturing process and fewer constraints on the material selection and structural design [15], [16]. Fused deposition modeling (FDM) and stereolithography apparatus (SLA) methods are the most commonly used 3D printing techniques for fabricating microwave devices [17]–[19]. The FDM method is used to create 3D objects by heating a thermoplastic filament and extruding it layer by layer [20]. The SLA method can be used to fabricate 3D objects with a liquid photopolymer resin that is cured and solidified by an ultraviolet laser [21]. The FDM method has a simpler process than the SLA method because it only requires a suitable extruder and printing bed temperature that depend on the filament. Thermoplastic filaments used in FDM include polylactic acid (PLA), acrylonitrile butadiene styrene (ABS), and Ninjaflex. Because of the easy process and low cost, these filaments are mainly used to manufacture microwave devices. For instance, a microstrip patch antenna using ABS (dielectric constant of $\varepsilon_r = 2.7$ and loss tangent of $\tan\delta = 0.01$), which exhibited a high gain and radiation efficiency at 7.5 GHz, was reported [22]. However, meshed wires had to be embedded in the ABS substrate to achieve adequate performance. Based on the flexibility and ease of use of Ninjaflex ($\varepsilon_r = 3.0$ and $\tan\delta = 0.05$), a bendable patch antenna for wearable applications [23] and bandwidth-enhanced substrate-integrated slab waveguide [24] were presented. In addition, a substrate-integrated waveguide (SIW) interconnect has been built with the 3D printing technology and a T-Glase filament [25]. However, the device performance parameters such as the antenna efficiency and insertion loss may degrade owing to the high dielectric loss of the 3D printing filament. In [26], the researchers have used a 3D-printed perforated structure and constructed a lightweight waveguide for RF applications. The X-band pyramidal horn antenna fabricated with the 3D metal direct printing technology achieved a gain of 9–13 dBi. Furthermore, an SIW with a 3D-printed honeycomb substrate with low insertion loss and high mechanical strength was reported [27]. However, there must be a trade-off between the insertion loss and mechanical strength in uniform perforated or honeycomb structures. For instance, a large unit cell can reduce insertion loss; however, its mechanical strength becomes weak. A smaller unit cell can achieve a high mechanical strength; however, the insertion loss and fabrication time are increased.

To solve this problem, an SIW fabricated on a non-uniform honeycomb substrate for minimizing the insertion losses caused by 3D-printing materials while maintaining mechanical strength is proposed. Because the planar SIW exploits the advantages of a microstrip circuit (i.e., the easy fabrication and compact size) and waveguide (i.e., the complete shielding and high power handling capability), it is suitable for implementing microwave components [28]. The honeycomb geometry is suitable for 3D-printed substrate designs because of its light weight, beneficial design, and structural strength [29]. In this study, a non-uniform honeycomb-shaped substrate composed of four differently sized honeycomb unit cells was designed to present the proposed concept. To reduce the volume of the 3D-printed substrate, large honeycomb unit cells were chosen for the non-uniform honeycomb-shaped substrate for the SIW and the transition sections. The low volume results in the low insertion loss of the SIW. The electrical properties of the non-uniform honeycomb substrate were characterized based on the honeycomb unit cell size. In addition, the insertion losses of the SIW, tapered transitions, and microstrip feed line sections were examined with respect to the honeycomb unit cell size. The performance characteristics of the SIW on the proposed non-uniform honeycomb-shaped structure were compared with those of SIWs on solid and uniform honeycomb-shaped structure. Finally, microstrip-fed SIWs were fabricated, and the proposed concept was numerically and experimentally evaluated with S-parameters.

II. SUBSTRATE-INTEGRATED WAVEGUIDE (SIW) DESIGN ON NON-UNIFORM HONEYCOMB-SHAPED SUBSTRATE

A. ELETRICAL PROPERTIES OF HONEYCOMB SUBSTRATE

Fig. 1 shows uniform honeycomb-shaped substrates with unit cells of different sizes. To realize the non-uniform honeycomb-shaped substrate, the electrical properties of the uniform honeycomb-shaped substrates with different unit cell sizes were characterized with an electromagnetic (EM) analysis.

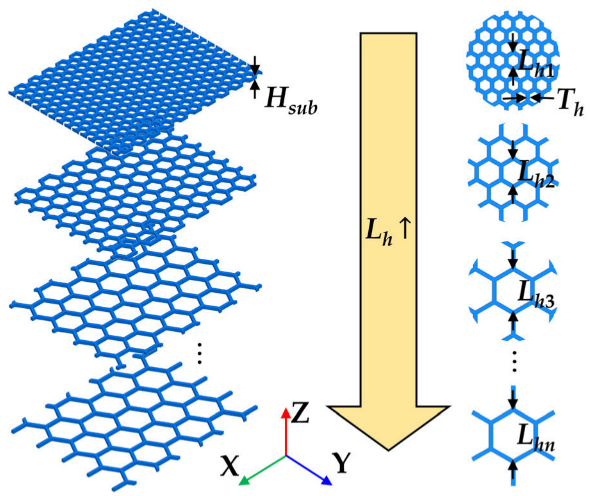

FIGURE 1. Schematic of PLA honeycomb substrate with differently sized unit cells (L_h: honeycomb unit cell size, T_h: honeycomb unit cell thickness, H_{sub}: substrate height).

The solid PLA substrate, which was printed with a 100% infill density, had a dielectric constant of $\varepsilon_r = 2.2$ and loss tangent of $\tan\delta = 0.05$ within the frequency range of 1–6 GHz [20]. When the substrate height H_{sub} increases, the effective dielectric constant decreases because of the increased fringing field effect of the transmission line [27]. The thicker substrate height and lower effective dielectric constant result in a wider microstrip line on the substrate. The wide microstrip line may increase the conductive loss and require an additional 50 Ω impedance matching circuit. Thus, the honeycomb substrate height H_{sub} was set to 1 mm.

In addition, the unit cell thickness T_h was fixed at 1 mm for stable 3D printing and parametric studies of the honeycomb unit cell size L_h. Two types of transmission line techniques were used to characterize the dielectric constant and dielectric loss of the honeycomb substrate. For a honeycomb unit cell size L_h of 4 mm or less, the dielectric constant and dielectric loss of the honeycomb substrate were determined with the microstrip transmission line technique [30]–[32]. Compared to the waveguide transmission line technique, the microstrip transmission line method can characterize the dielectric constant in a broader frequency band. Thus, the microstrip transmission line method was chosen for the honeycomb substrate with $L_h = 4$ mm or less. For a honeycomb unit cell size L_h that exceeds 4 mm, the dielectric constant and dielectric loss of the honeycomb substrate were determined with the waveguide transmission line technique [33], [34] because it is difficult to apply the microstrip transmission technique for honeycomb substrates with larger unit cells.

Fig. 2(a) shows the dielectric constant of the honeycomb substrate with respect to the frequency. The dielectric constants of the honeycomb-shaped substrate remain constant within the frequency range of 1–8 GHz. As the honeycomb unit cell size L_h increases from 3 to 12 mm, the dielectric constant ε_r of the substrate decreases from 1.5 to 1.01 (similar to that of air). In addition, the electrical properties of the honeycomb-shaped substrate depending on the honeycomb unit cell size at 3.5 GHz were investigated with EM simulations. With increasing L_h, the PLA volume of the honeycomb substrate, which has the same dimensions, decreases from 47% to 16.2%. This reduces the dielectric loss from 0.035 to 0.013, as shown in Fig. 2(b). The 50 Ω microstrip line width was designed for a microstrip feed line section on the honeycomb substrate. When the honeycomb unit cell size exceeds 3.5 mm, its effective dielectric constant and dielectric loss become lower than 1.3 and 0.03, respectively. However, the mechanical strength of the honeycomb-shaped substrate decreases because of the large honeycomb unit cell. Furthermore, the 50 Ω microstrip line width must exceed 4 mm, as shown in Fig 2(c). Because a wider microstrip line width may increase the conductive loss, the honeycomb unit cell size is 3 mm ($\varepsilon_r \approx 1.5$), which results in a 50 Ω microstrip line width of 3.75 mm.

B. SIW DESIGN ON HONEYCOMB SUBSTRATE

A transverse electric (TE_{10}) mode SIW with a cut-off frequency of 2.2 GHz was designed to study the insertion loss of the PLA honeycomb substrate. For the TE_{10} mode SIW, the cut-off frequency can be obtained from the following simplified equation [35]:

$$f_c = \frac{c}{2a_d\sqrt{\varepsilon_r}}, \tag{1}$$

where c is the speed of light in a vacuum, a_d is the dielectric filled SIW width, and ε_r is the dielectric constant of the SIW material. The diameter (D) of the metal via hole and via

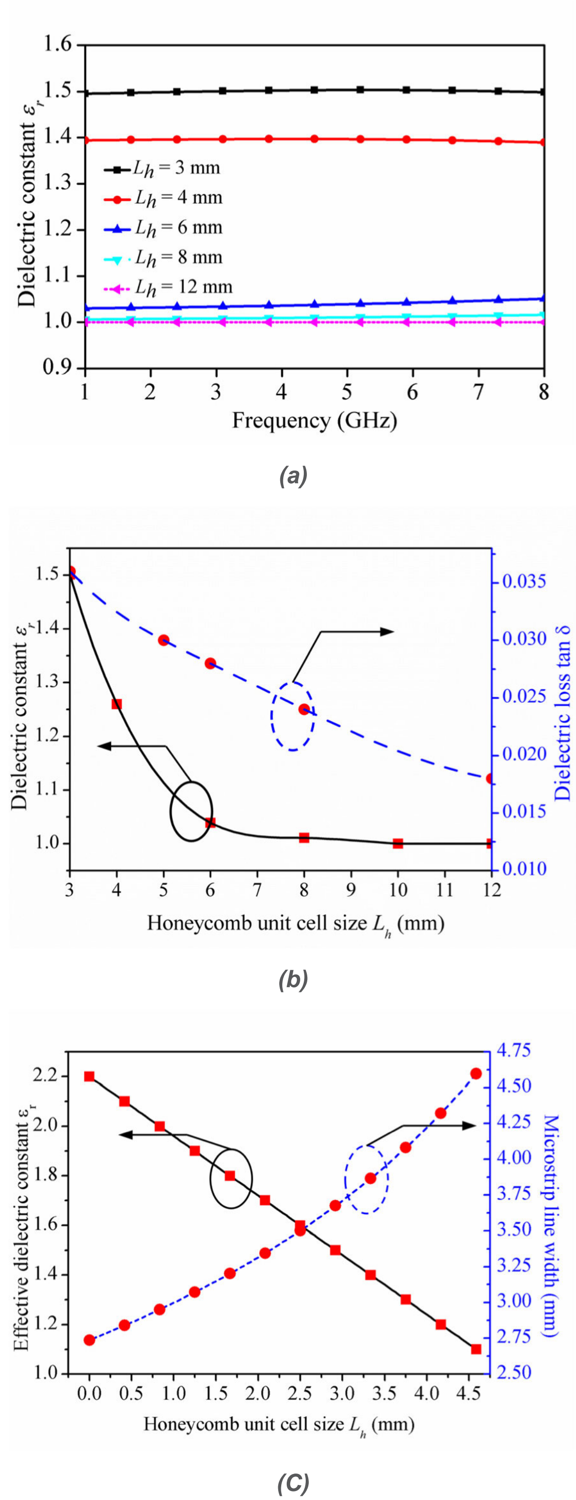

FIGURE 2. Electrical properties of honeycomb substrate with respect to (a) frequency and (b) length of honeycomb unit cell L_h; (c) 50 Ω microstrip line width with respect to effective dielectric constant.

pitch (P) of the SIW can be derived as follows [36]:

$$D < \frac{\lambda_g}{5}, \tag{2}$$

$$P < 2D, \tag{3}$$

where λ_g is the SIW cavity guided wavelength.

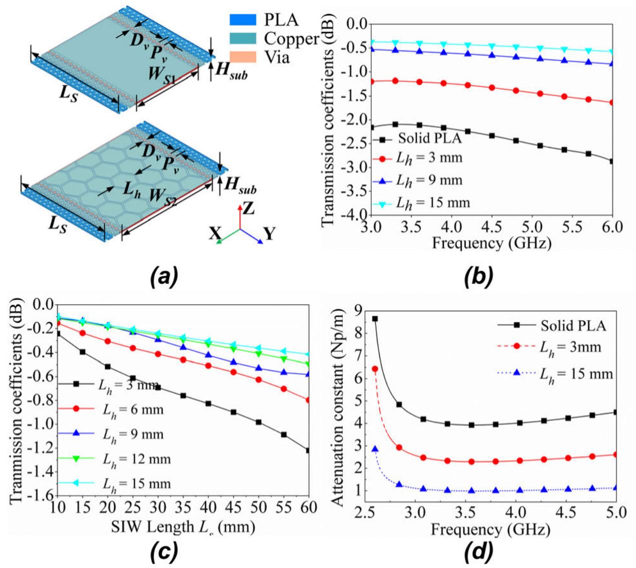

FIGURE 3. Simulated results of (a) SIW on solid PLA and honeycomb substrate, (b) transmission coefficients with respect to L_h and (c) L_s (d) attenuation constant.

Fig. 3(a) shows the TE_{10} mode SIWs on the solid and honeycomb-shaped substrates. The SIWs on the honeycomb-shaped substrates were designed with different unit cell sizes, and parametric studies were performed to investigate the respective insertion losses. The SIW length L_s, via diameter D_v, via pitch P_v, and substrate height H_{sub} are 64, 2.7, 3.17, and 1 mm for the SIW designs on the solid and honeycomb-shaped substrates, respectively. The SIW width W_s derived from (1) depends on the dielectric constant of the SIW material. Thus, the SIW width W_s was set to 48.5 mm for the solid PLA substrate ($\varepsilon_r = 2.2$) and to 68.5 mm for the honeycomb substrate with $L_h = 15$ mm ($\varepsilon_r = 1.01$). The honeycomb substrate formed by the 2.5 mm unit cell was combined with the SIW substrate to generate via walls. The average insertion loss of the SIW with the solid PLA substrate is 2.37 dB in the range of 3–6 GHz. When the L_S is 64 mm, and the L_h increases to 3, 9, and 15 mm, the average insertion losses of the SIW with the honeycomb substrate are 1.35, 0.67, and 0.46 dB, respectively, as shown in Fig. 3(b). Moreover, Fig. 3(c) shows the transmission coefficients with respect to the SIW length L_S. The insertion losses of the SIW with $L_h = 12$ and 15 mm decrease to 0.01 and 0.007 dB/mm; the average insertion loss of the SIW with $L_h = 3$ mm is 0.021 dB/mm. Fig. 3(d) shows the attenuation constant of the SIW with the solid PLA and honeycomb substrates with $L_h = 3$ and 15 mm. The attenuation constant of the SIW can be derived as follows [37]:

$$\alpha = \frac{k^2}{2\beta}\left(\tan\delta + \frac{2R_s}{\omega\mu h} + \frac{4\pi^2 R_s'}{\omega\mu k^2 {w_{eff}}^3}\right) \tag{4}$$

where k and β are the complex wave number in the substrate material and propagation constant, respectively; $\tan\delta$ is the dielectric loss of the substrate material; h and w_{eff} are the substrate thickness and equivalent width of the SIW, respectively; moreover, R_s and R_s' are the surface resistivity of the SIW top and bottom surface and equivalent surface resistivity of the via arrays, respectively. The insertion loss of the SIW is mainly affected by the dielectric loss of the substrate material. Thus, the attenuation constants of the honeycomb-shaped substrates decrease with increasing honeycomb unit cells. When the PLA volume in the honeycomb substrate decreases from 42.8% to 12.4%, the insertion losses of the SIW with the honeycomb substrate also decrease.

C. TAPERED TRANSITION DESIGN ON HONEYCOMB SUBSTRATE

The microstrip-fed SIW must be required to verify its insertion loss on the non-uniform honeycomb substrate. Therefore, SIWs with tapered transitions for the conversion between the quasi-transverse EM mode in the microstrip feed line and transverse electric (TE) mode in the SIW were designed. To design the transition section for the honeycomb substrate, the size of the honeycomb unit cell L_{hs} for the SIW area was 12 mm for low dielectric loss, and the size of the honeycomb unit cells L_{hm} for the microstrip line sections was 3 mm for 50 Ω impedance matching. Moreover, the via walls on the substrate were designed with 2.5 mm honeycomb unit cells. The transition width W_{tr} and length L_{tr} are determined by the dielectric constant of the honeycomb substrate; hence, the transition width and length were optimized in an EM analysis, as shown in Fig. 4(e).

The initial width of the taper transition was obtained with curve fitting and the analytical equation for the impedance of a microstrip line [38]:

$$\frac{1}{w_e} = \frac{4.38}{W_{SIW}}\exp\left(\frac{-0.627\varepsilon_r}{\frac{\varepsilon_r+1}{2} + \frac{\varepsilon_r-1}{2\sqrt{1+12H_{sub}/W_m}}}\right), \tag{5}$$

where W_{SIW} is the width of the SIW, ε_r the dielectric constant of the substrate, and H_{sub} and W_m are the substrate height and microstrip line width, respectively.

The initial transition length is commonly assumed to be a quarter wavelength of the operating frequency to minimize the return loss. Thus, parametric studies were performed to investigate the effects of the transition length L_{tr} and width W_{tr}, as shown in Fig. 4(a). Figs. 4(b) and (c) show the return and insertion losses for different transition lengths L_{tr} when $L_t = 6$ mm and $W_{tr} = 16.8$ mm. When L_{tr} increases from 18 to 26 mm, 50 Ω impedance matching is achieved at 3–6 GHz. Furthermore, the average insertion losses of the transition structures are 0.67, 0.55, and 0.57 dB, respectively. Fig. 4(d) shows the insertion losses of the transition structure on the honeycomb substrate for different unit cell sizes. When the honeycomb unit cell L_t of the transition sections is 3, 6, or 9 mm, the insertion loss of the transition structure is 0.71, 0.57, or 0.54 dB, respectively. Thus, large unit cells with $L_t = 6$ mm were used for the transition sections on the honeycomb substrate to reduce the insertion loss. In addition, the microstrip-fed SIW with optimized L_{tr} and W_{tr} was

TABLE 1. Design Parameters for SIW with Solid PLA, Uniform Honeycomb Substrate, and Non-Uniform Honeycomb Substrate (in mm).

Substrate type	W_{sub}	L_{sub}	W_{SIW}	L_{SIW}	H_{sub}	W_{tr}	L_{tr}	W_m
Solid PLA	70	85	42.5	25	1	9.2	16	3.2
Uniform honeycomb	73.3	81	47.9	25	1	12.8	19	3.8
Non-uniform honeycomb (case 1)	73.3	81	57.2	25	1	11.8	17.3	3.8
Non-uniform honeycomb (case 2)	81	86	57.2	25	1	17	23	3.8
Non-uniform honeycomb (case 3)	71.6	91	57.2	25	1	15.8	23	3.8

TABLE 2. Electrical Properties of Solid PLA, Uniform Honeycomb, and Non-uniform Honeycomb Substrates.

Characteristics	Solid PLA	Uniform honeycomb	Non-uniform honeycomb
Dielectric constant (ε_r)	2.2	1.5	1.27 (avg)
Loss tangent (tanδ)	0.05	0.035	0.024 (avg)

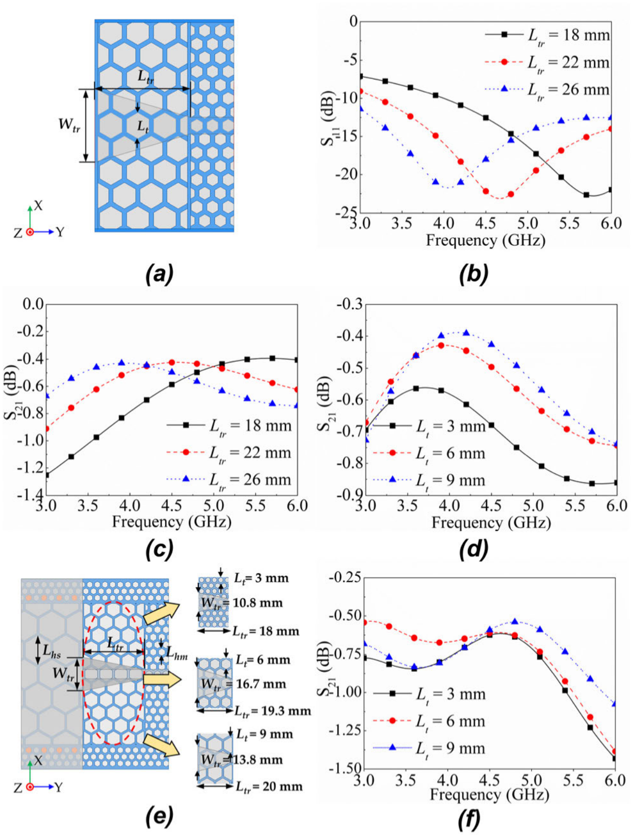

FIGURE 4. Simulated results of (a) transition with microstrip line; (b) S_{11} and (c) S_{21} with respect to different transition lengths for $L_t = 6$ mm; (d) S_{21} for different unit cell sizes of honeycomb substrate; (e) microstrip-fed SIW on non-uniform honeycomb substrate; (f) S_{21} with respect to L_t.

simulated to investigate the insertion loss depending on the unit cell size L_t of the transition substrate, as shown in Fig. 4(e). Fig. 4(f) shows the insertion losses of the microstrip-fed SIW for different L_t. When the L_t values for the transition substrate are 3, 6, and 9 mm, the average insertion losses of the microstrip-fed SIW on the non-uniform honeycomb substrate are 0.85, 0.76, and 0.74 dB, respectively. In the microstrip-fed SIW, the change in the average insertion loss based on the honeycomb unit cell size is smaller than that of the SIW because the microstrip line on the transition substrate is less susceptible to dielectric losses. In addition, the insertion loss of the microstrip-fed SIW increases slightly at 6 GHz owing to impedance matching.

D. DESIGN OF MICROSTRIP-FED SIW ON HONEYCOMB SUBSTRATE

Based on the parametric studies of the unit cell size of the honeycomb substrate, the microstrip-fed SIWs on the solid PLA, uniform honeycomb, and three types of non-uniform honeycomb substrates were simulated, as shown in Figs. 5(a), (c), (e), (g), and (i). Table 1 lists the geometrical parameters of the microstrip-fed SIWs for these five types of substrates. First, the substrate height H_{sub} was set to 1 mm for the easy fabrication and design of the microstrip feed line. Furthermore, the SIW length L_{SIW} was fixed to 25 mm ($\lambda_0/4$) for all types of microstrip-fed SIWs. The SIW width W_{SIW} was determined to be 42.5, 47.9, and 57.2 mm based on the dielectric constants of the substrates, respectively. The electrical properties of each substrate are summarized in Table 2. Because the non-uniform honeycomb-shaped substrate is composed of four differently sized honeycomb unit cells, the substrate has various dielectric constants from 1.03 to 1.5 and loss tangents from 0.013 to 0.035.

To examine the proposed non-uniform honeycomb substrate, microstrip-fed SIWs on three types of non-uniform substrates were designed. For cases 1 and 2, the non-uniform honeycomb substrates were designed with three differently sized honeycomb unit cells (3, 15, and 2.5 mm). For case 1, a honeycomb unit cell size of 15 mm was used for the SIW area on the substrate, and a honeycomb unit cell size of 3 mm was used for the two transitions and microstrip feed line sections. For case 2, uniform honeycomb unit cells of 15 mm were used for the SIW area and two transition sections. Subsequently, the microstrip feed line with honeycomb unit cells of 3 mm was designed on the substrate. For case 3 of the non-uniform honeycomb substrates, four differently sized honeycomb unit cells (3, 6, 12, and 2.5 mm)

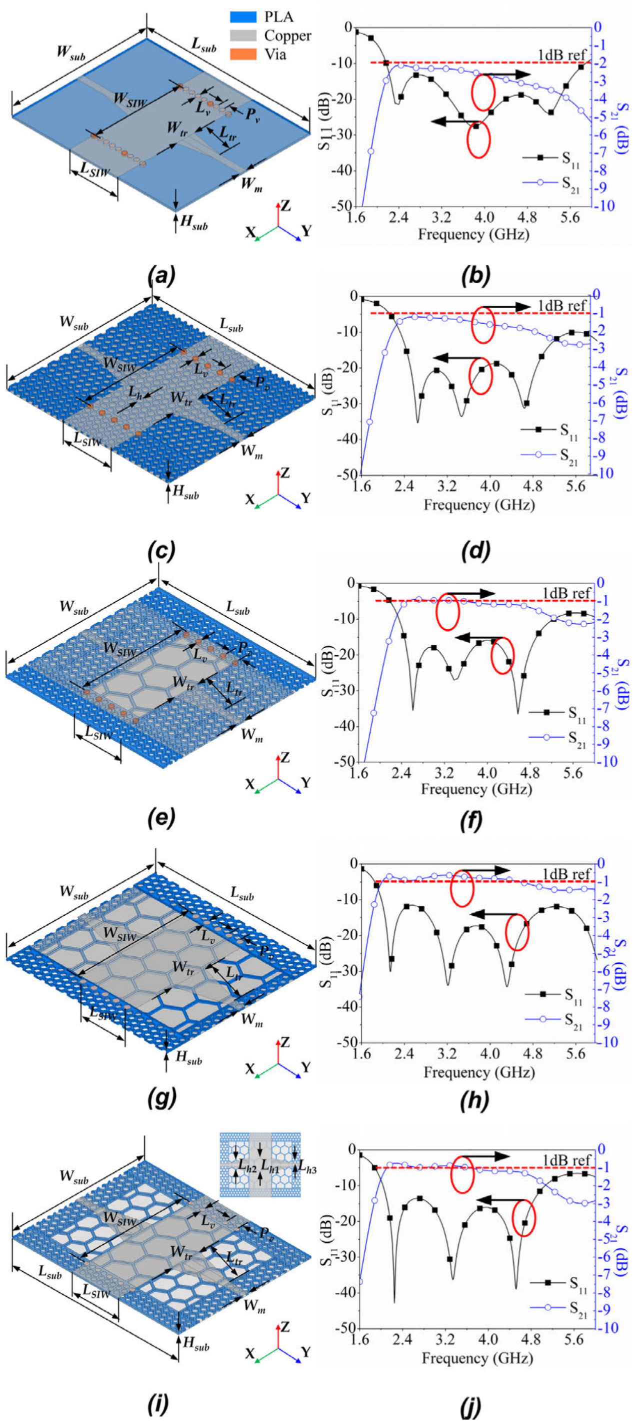

FIGURE 5. Simulated results of microstrip-fed SIW with (a) solid PLA, (c) uniform honeycomb substrate, (e) non-uniform honeycomb substrate (case 1), (g) non-uniform honeycomb substrate (case 2), (i) non-uniform honeycomb substrate (case 3); scattering parameters of SIW on (b) solid PLA substrate, (d) uniform honeycomb, (f) non-uniform honeycomb (case 1), (h) non-uniform honeycomb (case 2), (j) non-uniform honeycomb (case 3).

were chosen for the microstrip feed line, two transition sections, SIW area, and via walls, respectively. Regarding the uniform honeycomb substrate, a 3 mm unit cell structure was applied for the easy printing and design of the microstrip feed line. Figs. 5(b), (d), (f), (h), and (j) show the simulated S-parameters of the microstrip-fed SIWs of each substrate. The simulated 10 dB bandwidths of the microstrip-fed SIWs of the solid PLA and uniform and three types of non-uniform honeycomb substrates are 3.7, 3.23, 2.93, 4.1, and 3.05 GHz, respectively. The average insertion loss of the SIW with the solid PLA substrate is 2.45 dB, and that of the SIW with the uniform honeycomb substrate is 1.42 dB at 2–4 GHz. However, the average insertion losses of the SIWs with three types of non-uniform honeycomb substrates are decreased to 1.38, 0.76, and 1.02 dB in the same frequency range. Moreover, the insertion losses with respect to the lengths of all SIWs are 0.029, 0.018, 0.017, 0.009, and 0.011 dB/mm, respectively. Therefore, low-loss SIW could be achieved with the non-uniform honeycomb substrates of cases 2 and 3.

A large cell size of the honeycomb unit is generally preferred for SIWs because of the lower dielectric loss. However, the top conductive layer on the SIW is unstable in the case of large honeycomb cells. Thus, to achieve low insertion loss and robustness, the large cells were implemented at the center where the electric field is strong. In addition, medium cells were chosen for the sides for robustness, and the cell size of the honeycomb in the microstrip section was adjusted according to low insertion loss and high robustness. Moreover, the edges for the vias were constructed with small unit cells. Therefore, the final non-uniform honeycomb substrate was composed of four differently sized honeycomb unit cells for each section: L_{h1} of the SIW area was 12 mm, and L_{h2} of the two transition sections was 6 mm. The honeycomb unit cell of $L_{h3} = 3$ mm was used for the two microstrip feed line sections, which was determined by the characteristic impedance of the microstrip line on the substrate. The via walls were built on the honeycomb substrate with unit cells L_v of 2.5 mm.

Figs. 6(a)–(f) show the electric and magnetic field distributions of the TE_{10} mode SIWs on the non-uniform and uniform honeycomb substrates at 3.5 GHz, respectively. The SIW supports only the TE mode because the surface currents are interrupted by the via walls of the SIW in the transverse magnetic mode. For the TE_{10} mode SIW, the electric field is in the x-y plane (E_z), and the magnetic field is in the y-z plane (H_x) and z-x plane (H_y). The magnitudes of E_z and H_y are determined by the cut-off wavenumber, which is related to the SIW width [35]. Therefore, the magnitudes of E_z and H_y of the SIW with the non-uniform honeycomb substrate are slightly lower than those of the uniform honeycomb substrate; the magnitude of H_x is unaffected by the SIW width and similar for both substrates, as shown in Fig. 6. The reflection responses can be improved because of the similar field distributions of the SIW and microstrip on the designed substrate.

Fig. 7 shows the fabrication error analysis results of the via insertion, transition length, and width. The manual insertion of the metal vias causes a gap between the 3D-printed substrate and metal vias, which ultimately leads to a reduction in

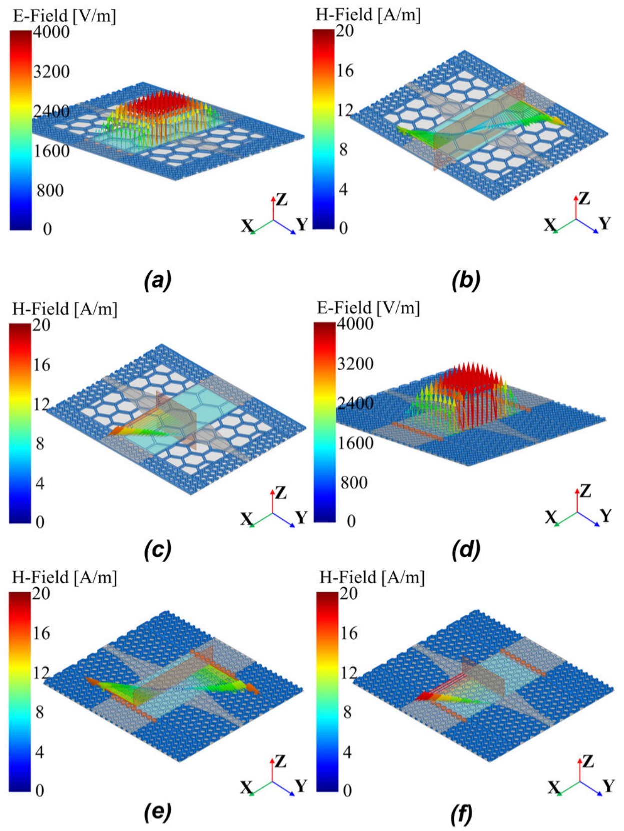

FIGURE 6. Simulated results of TE_{10} mode SIW field distribution at 3.5 GHz: (a) E_Z on x-y plane, (b) H_Y on z-x plane, (c) H_X on y-z plane for non-uniform honeycomb substrate; (d) E_Z on x-y plane, (e) H_Y on z-x plane, and (f) H_X on y-z plane for uniform honeycomb substrate.

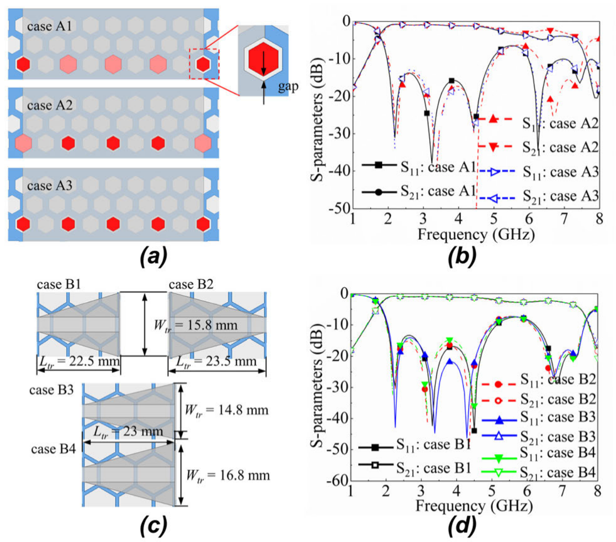

FIGURE 7. Fabrication error analysis of: (a) via insertion, (b) S-parameters of each case; (c) transition length and width, (d) S-parameters of each case.

the bandwidth. To analyze the tolerance, three cases were discussed: corner vias denoted as ''case 1'', center vias denoted as ''case 2'', and all vias denoted as ''case 3'', as illustrated in Fig. 7(a). The tapered transition length and width can be slightly different from the expected geometry. Fig. 7(c) presents the effects of this tolerance on the S-parameters. The effect of the transition length difference (22.5 and 23.5 mm) was analyzed for cases B1 and B2. Furthermore, the effect of the transition width difference (14.8 and 16.8 mm) was analyzed for cases B3 and B4. Evidently, the S_{11} results have slight differences depending on the transition length and width.

III. RESULTS AND DISCUSSION

The microstrip-fed SIWs were deposited on uniform and non-uniform honeycomb substrates to study experimentally the performance of the proposed SIW. Fig. 8 shows the fabricated microstrip-fed SIWs on the 3D-printed uniform and non-uniform honeycomb substrates. The widths of the uniform and non-uniform honeycomb substrates were 75.3 and 72.6 mm, respectively. The total length of the uniform honeycomb substrate, including the microstrip line at both ends, was 83 mm; that of the non-uniform honeycomb substrate was 91 mm.

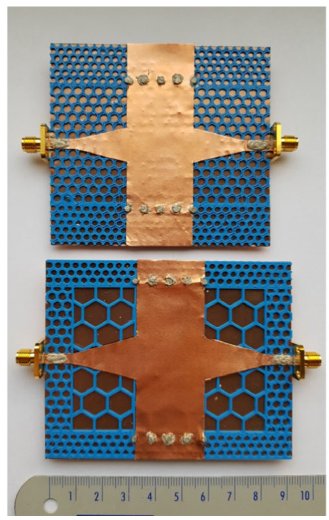

FIGURE 8. Fabricated 3D-printed microstrip-fed SIWs with uniform (top) and non-uniform (bottom) honeycomb substrates.

Moreover, a PLA filament provided by ColorFabb® (Belfeld, The Netherlands) was used to 3D-print the substrate. The PLA filament requires a temperature of 210 °C for the extrusion nozzle and 50 °C for the print bed; thus, it is less sensitive than other thermoplastic filaments. Hence, the prototype of the 3D-printed substrate can be easily and rapidly fabricated. In addition, PLA filaments are biodegradable, which enables the environmentally friendly fabrication of prototypes [39]. Because of their mechanical properties such as the flexibility and light weight, PLA filaments are suitable for the dielectric materials of microwave circuits. The conductive patterns for the microstrip-fed SIWs were deposited on the 3D-printed substrates with adhesive copper films. The brass via pins, the diameters of which were 2.5 mm, were

TABLE 3. Performance Comparison of SIWs fabricated on Uniform and Non-uniform Honeycomb Substrates.

Parameter	Uniform honeycomb	Non-uniform honeycomb
Average insertion loss (dB)	1.38	0.92
Insertion loss (dB/mm)	0.018	0.010
10 dB bandwidth (GHz)	2.65	2.3
Substrate weight (g)	3.06	2.28
Overall weight (g)	13.76	12.38
Substrate size (W mm × L mm× H mm)	75.3 × 83.1 × 1	72.6 × 91 × 1
Printing time (min)	32	17

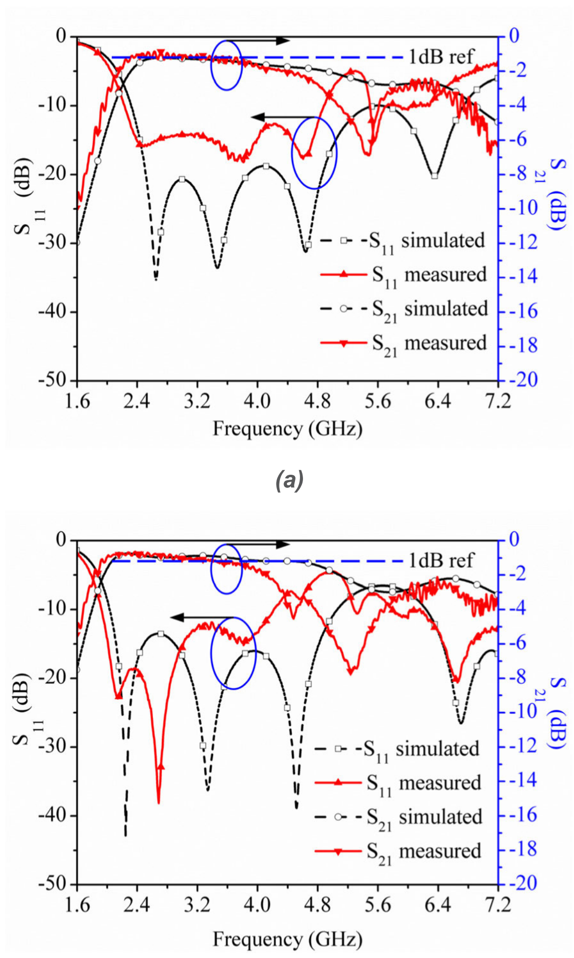

FIGURE 9. Simulated and measured results of SIWs for (a) uniform and (b) non-uniform honeycomb substrates.

inserted into the 3D-printed substrates to generate the via walls of the SIWs. Moreover, subminiature version A (SMA) connectors were mounted on the substrate to measure the S-parameters of the microstrip-fed SIWs; the via pins and SMA connectors were fixed onto the substrates with silver epoxy.

Fig. 9 shows the simulated and measured results of the two fabricated samples. The simulated and measured average insertion losses of the microstrip-fed SIW on the non-uniform honeycomb substrate are 0.96 and 0.92 dB in the range of 1.97–3.35 GHz, respectively, whereas the simulated and measured average insertion losses of the microstrip-fed SIW on the uniform honeycomb substrate are 1.74 and 1.38 dB for the same frequency range, respectively. Furthermore, the insertion loss of the microstrip-fed SIW on the non-uniform honeycomb substrate is 0.010 dB/mm, whereas that of the microstrip-fed SIW on the uniform honeycomb substrate is 0.018 dB/mm. Thus, the proposed non-uniform honeycomb substrate exhibits a good insertion loss performance. The simulated 10 dB bandwidths of the microstrip-fed SIWs for the uniform and non-uniform honeycomb substrates are 3.23 and 3.05 GHz, whereas the measured 10 dB bandwidths of the microstrip-fed SIWs for the two substrates are 2.65 and 2.3 GHz, respectively. Because of the via hole fabrication tolerance, the measured 10 dB bandwidth results of both microstrip-fed SIWs are decreased. Although the simulated and measured results of the microstrips agree well, they exhibit a slight difference because the conductive pattern and inserted via pins for the via walls were manually prepared. In addition, because the material was characterized at 3.5 GHz, the difference between the simulation and measurement results is greater at higher frequencies.

Table 3 compares the performance of the microstrip-fed SIWs fabricated on uniform and non-uniform honeycomb substrates. Large honeycomb unit cells reduce the dielectric constant and dielectric loss of the honeycomb substrate. Consequently, the wavelength of the SIW for the non-uniform honeycomb substrate increases. As shown in Table 3, the total sizes of the devices may be increased. However, the average insertion loss of the microstrip-fed SIW for the proposed non-uniform honeycomb substrate is reduced by 22.1% compared to that of the uniform honeycomb substrate. The microstrip-fed SIWs on these two types of substrates achieve broad bandwidths of over 2 GHz, which can be used for various S-band applications. The overall weight of the microstrip-fed SIW on the non-uniform honeycomb substrate, including those of the SMA connector and via, is only 12.38 g; moreover, the thin 3D-printed substrate of 1 mm thickness simplifies the realization of a planar configuration. Regarding the manufacture, the non-uniform honeycomb substrate can reduce the printing time by 50% compared to the uniform substrate. Furthermore, the proposed non-uniform honeycomb substrate is more cost-effective than the uniform substrate because it requires less filament.

TABLE 4. Comparison of Proposed and Common SIW Transmission Lines.

	Center Frequency (GHz)	Relative Length	Material (tan δ)	Fabrication method	Insertion loss (dB/mm)	Fractional Bandwidth(%)	Cost
This work	2.6	$0.9\lambda_g$	PLA (0.05)	3D printing	0.010	92.3	Very low
[7]	10	$1.2\lambda_g$	PCB (0.0009)	Machining	0.061	55	High
[8]	15	$8\lambda_g$	FR-4 (0.02)	Machining	0.045	40	Average
[9]	32	$6.9\lambda_g$	RT6002 (0.0012)	Machining	0.010	43.8	High
[10]	14	$5\lambda_g$	RO4003(0.0012)	Machining	0.019	82	High
[24]	4.5	$2.2\lambda_g$	Ninjaflex (0.05)	3D printing	N/A	66.7	Average
[25]	4.5	$0.5\lambda_g$	T-Glase (0.01)	3D printing	0.086*	38	Average
[27]	4.5	$1.3\lambda_g$	PLA (0.05)	3D printing	0.020	101	Very low
[40]	2.75	$0.7\lambda_g$	Rubber, Taffeta (0.015)	Manual	0.021	67.2	Low
[41]	32	$0.6\lambda_g$	Fused silica (0.0003)	Semi-additive patterning	0.018	15.6	High

* This data is estimated from figures.

Table 4 compares the proposed and other SIW transmission lines. A folded SIW with compact size and a double layer PCB substrate and a SIW interconnect for 3D integration with commercial PCB were reported in [7], [8]. In [9], [10], an air-filled SIW made of a multi-layer printed circuit and ridge empty SIW for low losses in broadband applications were presented. These SIW transmission lines can be applied to the high-frequency range. However, the conventional PCB fabrication process is more complicated than 3D printing. In this study, the honeycomb-shaped structure resulted in a low insertion loss (0.01 dB/mm) and reduced the effective dielectric loss (0.018). The insertion loss of the SIW proposed in [7] is higher than that of the proposed SIW because of the multi-layer and folded SIW configuration used for miniaturization in [7]. Moreover, broadband SIWs and SIW interconnect have been produced with 3D printing. Those prototypes could not reduce the insertion loss because of the high dielectric loss of the 3D printing filament. In [40], [41], SIWs with various materials such as conductive textile and fused silica were proposed. In addition, a folded SIW for wearable electronics with closed-cell expanded rubber and the conductive textile Taffeta was presented. However, all prototypes had to be fabricated manually. Furthermore, a SIW on a glass-based substrate for mm-wave applications was created. It is obvious that PCB is mechanically stronger than plastics such as PLA and ABS. The proposed microstrip-fed SIW exhibits low insertion loss and sufficient bandwidth at low operating frequencies compared to other SIW transmission lines. In addition, its fabrication with 3D printing is easy, fast, and inexpensive.

IV. CONCLUSION

Three-dimensional (3D)-printed structures are inexpensive, easy to produce, and lightweight. However, filament materials used for 3D printing are lossy at high frequencies. Therefore, a novel honeycomb-shaped substrate for minimizing the dielectric loss and maintaining the mechanical strength is proposed. More specifically, large honeycomb unit cells were chosen for the SIW and transition sections on the non-uniform honeycomb-shaped substrate. The volume of the non-uniform honeycomb-shaped substrate is reduced by 65% and 26% compared to those of a solid PLA substrate and uniform honeycomb-shaped substrate. In addition, the SIW on the non-uniform honeycomb-shaped substrate exhibits low insertion loss because of the low substrate volume.

According to the numerical and experimental study results, the proposed non-uniform honeycomb substrate reduces the dielectric loss of the 3D-printed structure fabricated with PLA filaments. Moreover, the proposed microstrip-fed SIW for non-uniform honeycomb substrates was compared with that for uniform substrates. The average insertion loss of the microstrip-fed SIW with the non-uniform honeycomb substrate decreases to 0.92 dB at 1.97–3.35 GHz, which is comparable to that of the SIW fabricated on a commercial PCB. The 10 dB bandwidth of the proposed SIW for the non-uniform substrate is approximately 2.3 GHz in the microwave frequency range of 1.92–4.22 GHz. In addition, the proposed non-uniform honeycomb structure results in a 10% reduction in the weight and 50% reduction in the printing time. Although the conductive pattern of the SIW on the 3D-printed substrate requires additional post-processing, the proposed SIW can be easily, rapidly, and cost-effectively realized with 3D printing. Based on these advantages, the 3D-printed non-uniform honeycomb substrates may be interesting candidates for the manufacture of various RF components such as antennas, filters, and sensors, particularly for S-band applications. Moreover, the proposed SIW is suitable for space applications owing to its lightweight. A multi-material electronic 3D printer capable of 3D-printing PLA and conductive silver inks has recently been presented. This 3D printer enables the creation of true 3D printing structures without post-processing for conductive patterns [42]. Owing to the technical progress of multi-material printers and conductive filaments, the application of the proposed structure may be extended to 3D-printed RF systems.

REFERENCES

[1] T. D. Ngo, A. Kashani, G. Imbalzano, K. T. Q. Nguyen, and D. Hui, "Additive manufacturing (3D printing): A review of material, methods, applications and challenges," *Compos. B, Eng.*, vol. 143, pp. 172–196, Jun. 2018.

[2] J.-Y. Lee, J. An, and C. K. Chua, "Fundamentals and applications of 3D printing for novel materials," *Appl. Mater. Today*, vol. 7, pp. 120–133, Jun. 2017.

[3] B. Zhang, B. Seong, V. Nguyen, and D. Byun, "3D printing of high-resolution PLA-based structures by hybrid electrohydrodynamic and fused deposition modeling techniques," *J. Micromech. Microeng.*, vol. 26, no. 2, pp. 1–8, 2016.

[4] M. S. Mannoor, Z. Jiang, T. James, Y. L. Kong, K. A. Malatesta, W. O. Soboyejo, N. Verma, D. H. Gracias, and M. C. McAlpine, "3D printed bionic ears," *Nano Lett.*, vol. 13, no. 6, pp. 2634–2639, Jun. 2013.

[5] A. Au, W. Huynh, L. Horowitz, and A. Folch, "3D printed microfluidics," *Angew. Chemie-Int. Ed.*, vol. 55, no. 12, pp. 3862–3881, 2016.

[6] C. Zhu, T. Liu, F. Qian, W. Chen, S. Chandrasekaran, B. Yao, Y. Song, E. B. Duoss, J. D. Kuntz, C. M. Spadaccini, M. A. Worsley, and Y. Li, "3D printed functional nanomaterials for electrochemical energy storage," *Nano Today*, vol. 15, pp. 107–120, Aug. 2017.

[7] N. Grigoropoulos, B. Sanz-Izquierdo, and P. R. Young, "Substrate integrated folded waveguides (SIFW) and filters," *IEEE Microw. Wireless Compon. Lett.*, vol. 15, no. 12, pp. 829–831, Dec. 2005.

[8] A. Suntives and R. Abhari, "Transition structures for 3-D integration of substrate integrated waveguide interconnects," *IEEE Microw. Wireless Compon. Lett.*, vol. 17, no. 10, pp. 697–699, Oct. 2007.

[9] F. Parment, A. Ghiotto, T.-P. Vuong, J.-M. Duchamp, and K. Wu, "Air-filled substrate integrated waveguide for low-loss and high power-handling millimeter-wave substrate integrated circuits," *IEEE Trans. Microw. Theory Techn.*, vol. 63, no. 4, pp. 1228–1238, Apr. 2015.

[10] D. Herraiz, H. Esteban, J. A. Martinez, A. Belenguer, and V. Boria, "Microstrip to ridge empty substrate-integrated waveguide transition for broadband microwave applications," *IEEE Microw. Wireless Compon. Lett.*, vol. 30, no. 3, pp. 257–260, Mar. 2020.

[11] M. T. Sebastian and H. Jantunen, "Low loss dielectric materials for LTCC applications: A review," *Int. Mater. Rev.*, vol. 53, no. 2, pp. 57–90, Mar. 2008.

[12] A. E. I. Lamminen, J. Saily, and A. R. Vimpari, "60-GHz patch antennas and arrays on LTCC with embedded-cavity substrates," *IEEE Trans. Antennas Propag.*, vol. 56, no. 9, pp. 2865–2874, Sep. 2008.

[13] K. Qian, L. Zhao, and K.-L. Wu, "An LTCC coupled resonator decoupling network for two antennas," *IEEE Trans. Microw. Theory Techn.*, vol. 63, no. 10, pp. 3199–3207, Oct. 2015.

[14] S. H. Mousavi and A. B. Kouki, "High-SRF VHF/UHF lumped elements in LTCC," *IEEE Microw. Wireless Compon. Lett.*, vol. 25, no. 1, pp. 25–27, Jan. 2015.

[15] E. Macdonald, R. Salas, D. Espalin, M. Perez, E. Aguilera, D. Muse, and R. B. Wicker, "3D printing for the rapid prototyping of structural electronics," *IEEE Access*, vol. 2, pp. 234–242, Dec. 2014.

[16] S. Alkaraki and Y. Gao, "Mm-wave low-cost 3D printed MIMO antennas with beam switching capabilities for 5G communication systems," *IEEE Access*, vol. 8, pp. 32531–32541, 2020.

[17] R. Bahr, B. Tehrani, and M. M. Tentzeris, "Exploring 3-D printing for new applications: Novel inkjet- and 3-D-printed millimeter-wave components, interconnects, and systems," *IEEE Microw. Mag.*, vol. 19, no. 1, pp. 57–66, Jan. 2018.

[18] M. I. M. Ghazali, S. Karuppuswami, A. Kaur, and P. Chahal, "3-D printed air substrates for the design and fabrication of RF components," *IEEE Trans. Compon., Packag., Manuf. Technol.*, vol. 7, no. 6, pp. 982–989, Jun. 2017.

[19] M. Dionigi, C. Tomassoni, G. Venanzoni, and R. Sorrentino, "Simple high-performance metal-plating procedure for stereolithographically 3-D-printed waveguide components," *IEEE Microw. Wireless Compon. Lett.*, vol. 27, no. 11, pp. 953–955, Nov. 2017.

[20] K. Prashantha and F. Roger, "Multifunctional properties of 3D printed poly(lactic acid)/graphene nanocomposites by fused deposition modeling," *J. Macromolecular Sci., A*, vol. 54, no. 1, pp. 24–29, Jan. 2017.

[21] C. Liu, Y. Zhang, and Y. Li, "Precisely manipulated origami for consecutive frequency reconfigurable antennas," *Smart Mater. Struct.*, vol. 28, no. 9, pp. 1–29, 2019.

[22] M. Liang, C. Shemelya, E. MacDonald, R. Wicker, and H. Xin, "3-D printed microwave patch antenna via fused deposition method and ultrasonic wire mesh embedding technique," *IEEE Antennas Wireless Propag. Lett.*, vol. 14, pp. 1346–1349, 2015.

[23] S. Moscato, R. Bahr, T. Le, M. Pasian, M. Bozzi, L. Perregrini, and M. M. Tentzeris, "Infill-dependent 3-D-Printed material based on NinjaFlex filament for antenna applications," *IEEE Antennas Wireless Propag. Lett.*, vol. 15, pp. 1506–1509, 2016.

[24] E. Massoni, L. Silvestri, G. Alaimo, S. Marconi, M. Bozzi, L. Perregrini, and F. Auricchio, "3-D printed substrate integrated slab waveguide for single-mode bandwidth enhancement," *IEEE Microw. Wireless Compon. Lett.*, vol. 27, no. 6, pp. 536–538, Jun. 2017.

[25] S. Moscato, R. Bahr, L. Perregrini, T. Le, M. M. Tentzeris, M. Pasian, and M. Bozzi, "Additive manufacturing of 3D substrate integrated waveguide components," *Electron. Lett.*, vol. 51, no. 18, pp. 1426–1428, Sep. 2015.

[26] G.-L. Huang, S.-G. Zhou, C.-Y.-D. Sim, T.-H. Chio, and T. Yuan, "Lightweight perforated waveguide structure realized by 3-D printing for RF applications," *IEEE Trans. Antennas Propag.*, vol. 65, no. 8, pp. 3897–3904, Aug. 2017.

[27] Y. Kim, M. M. Tentzeris, and S. Lim, "Low-loss and light substrate integrated waveguide using 3D printed honeycomb structure," *Materials*, vol. 12, no. 3, pp. 1–10, 2019.

[28] G. Venanzoni, D. Mencarelli, A. Morini, M. Farina, and F. Prudenzano, "Review of substrate integrated waveguide circuits for beam-forming networks working in X-band," *Appl. Sci.*, vol. 9, no. 5, pp. 1–19, 2019.

[29] L. Wang, K. Saito, Y. Gotou, and Y. Okabe, "Design and fabrication of aluminum honeycomb structures based on origami technology," *J. Sandwich Struct. Mater.*, vol. 21, no. 4, pp. 1224–1242, May 2019.

[30] P. I. Deffenbaugh, T. M. Weller, and K. H. Church, "Fabrication and microwave characterization of 3-D printed transmission lines," *IEEE Microw. Wireless Compon. Lett.*, vol. 25, no. 12, pp. 823–825, Dec. 2015.

[31] P. M. Narayanan, "Microstrip transmission line method for broadband permittivity measurement of dielectric substrates," *IEEE Trans. Microw. Theory Techn.*, vol. 62, no. 11, pp. 2784–2790, Nov. 2014.

[32] F. Pizarro, R. Salazar, E. Rajo-Iglesias, M. Rodriguez, S. Fingerhuth, and G. Hermosilla, "Parametric study of 3D additive printing parameters using conductive filaments on microwave topologies," *IEEE Access*, vol. 7, pp. 106814–106823, 2019.

[33] P. I. Deffenbaugh, R. C. Rumpf, and K. H. Church, "Broadband microwave frequency characterization of 3-D printed materials," *IEEE Trans. Compon., Packag., Manuf., Technol.*, vol. 3, no. 12, pp. 2147–2155, Dec. 2013.

[34] M. D. Janezic and J. A. Jargon, "Complex permittivity determination from propagation constant measurements," *IEEE Microw. Guided Wave Lett.*, vol. 9, no. 2, pp. 76–78, 1999.

[35] D. Pozar, *Microwave Engineering*, 4th ed. Hoboken, NJ, USA: Wiley, 2011, pp. 110–117.

[36] F. Xu and K. Wu, "Guided-wave and leakage characteristics of substrate integrated waveguide," *IEEE Trans. Microw. Theory Techn.*, vol. 53, no. 1, pp. 66–73, Jan. 2005.

[37] X.-C. Zhu, W. Hong, K. Wu, K.-D. Wang, L.-S. Li, Z.-C. Hao, H.-J. Tang, and J.-X. Chen, "Accurate characterization of attenuation constants of substrate integrated waveguide using resonator method," *IEEE Microw. Wireless Compon. Lett.*, vol. 23, no. 12, pp. 677–679, Dec. 2013.

[38] D. Deslandes, "Design equations for tapered microstrip-to-substrate integrated waveguide transitions," in *IEEE MTT-S Int. Microw. Symp. Dig.*, May 2010, pp. 704–707.

[39] G. Boussatour, P.-Y. Cresson, B. Genestie, N. Joly, and T. Lasri, "Dielectric characterization of polylactic acid substrate in the frequency band 0.5–67 GHz," *IEEE Microw. Wireless Compon. Lett.*, vol. 28, no. 5, pp. 374–376, May 2018.

[40] R. Moro, S. Agneessens, H. Rogier, A. Dierck, and M. Bozzi, "Textile microwave components in substrate integrated waveguide technology," *IEEE Trans. Microw. Theory Techn.*, vol. 63, no. 2, pp. 422–432, Feb. 2015.

[41] A. O. Watanabe, B. K. Tehrani, T. Ogawa, P. M. Raj, M. M. Tentzeris, and R. R. Tummala, "Ultralow-loss substrate-integrated waveguides in glass-based substrates for millimeter-wave applications," *IEEE Trans. Compon., Packag., Manuf., Technol.*, vol. 10, no. 3, pp. 531–533, Mar. 2020.

[42] A. Vallecchi, D. Cadman, W. G. Whittow, J. Vardaxoglou, E. Shamonina, and C. J. Stevens, "3-D printed bandpass filters with coupled vertically extruded split ring resonators," *IEEE Trans. Microw. Theory Techn.*, vol. 67, no. 11, pp. 4341–4352, Nov. 2019.